AGU PUBLICATIONS

JGR

Journal of Geophysical Research: Oceans

RESEARCH ARTICLE

10.1002/2016JC012066

Isotope constraints on seasonal dynamics of dissolved and particulate N in the Pearl River Estuary, south China

Feng Ye[1,2], Guodong Jia[1,3], Luhua Xie[1,2], Gangjian Wei[2], and Jie Xu[4]

[1]Key Laboratory of Ocean and Marginal Sea Geology, Guangzhou Institute of Geochemistry, Chinese Academy of Sciences, Guangzhou, China, [2]State Key Laboratory of Isotope Geochemistry, Guangzhou Institute of Geochemistry, Chinese Academy of Sciences, Guangzhou, China, [3]State Key Laboratory of Marine Geology, Tongji University, Shanghai, China, [4]State Key Laboratory of Tropical Oceanography, South China Sea Institute of Oceanology, Chinese Academy of Sciences, Guangzhou, China

Key Points:
- $\delta^{15}N$ (and $\delta^{18}O$) of NO_3^-, NH_4^+, and PN in the Pearl River Estuary were determined
- Different degrees of biological processing occurred between winter and summer
- Atmospheric NO_3^- input to the coastal PRE is significant during the winter season

Correspondence to:
G. Jia,
jiagd@gig.ac.cn

Citation:
Ye, F., G. Jia, L. Xie, G. Wei, and J. Xu (2016), Isotope constraints on seasonal dynamics of dissolved and particulate N in the Pearl River Estuary, south China, *J. Geophys. Res. Oceans*, *121*, 8689–8705, doi:10.1002/2016JC012066.

Received 17 JUN 2016
Accepted 26 OCT 2016
Accepted article online 2 NOV 2016
Published online 15 DEC 2016

Abstract Isotope measurements were performed on dissolved NO_3^-, NH_4^+, and suspended particulate total N along a salinity gradient in the Pearl River Estuary (PRE) to investigate seasonal changes in main N sources and its biogeochemical processing under the influence of monsoon climate. Our data revealed that municipal sewage and remineralized soil organic N were the major sources of DIN (NO_3^- and/or NH_4^+) in freshwater during winter and summer, respectively, whereas phytoplankton biomass was a major component of PN in both seasons. In low-salinity waters (<2–3), nitrification was proved to be a significant NO_3^- source via NH_4^+ consumption, with N isotope effects of −15.3‰ in summer and −23.7‰ in winter for NH_4^+ oxidation. The contribution of nitrification to the total NO_3^- pool was smaller in summer than in winter, most likely due to freshwater dilution. At midsalinities (3–20), $\delta^{15}N$ values of PN were similar to those of NO_3^- and NH_4^+ in summer, reflecting a strong coupling between assimilation and remineralization. In winter, however, higher $\delta^{15}N_{NH4}$ but lower $\delta^{15}N_{NO3}$ than $\delta^{15}N_{PN}$ were observed, even though $\delta^{15}N_{PN}$ was similar between summer and winter. Intense sediment-water interaction and resuspension of sediments during winter appeared largely responsible for the decoupling. At high salinities, the greater enrichment in $\delta^{18}O_{NO3}$ than in $\delta^{15}N_{NO3}$ (up to 15.6‰) in winter suggests that atmospheric deposition may contribute to NO_3^- delivery during the dry season. Overall, these results show the importance of seasonal variability in physical forcing on biological N sources and its turnover processes in the highly dynamic river-dominated estuary.

1. Introduction

As a transition zone between land and ocean, estuaries are characterized by strong gradients in environmental and ecological parameters. The behavior of nitrogen (N), one of the major and often limiting nutrient for primary production, in such a zone is complex, due partially to dynamic interactions between physical, chemical, and biological processes that govern the fate of N [*Wankel et al.*, 2007; *Dähnke et al.*, 2008]. In addition, the time-varying and/or multiple N sources that are closely associated with human activities in recent decades make it more difficult to understand N behavior in an estuary.

Among many methods, stable nitrogen isotope ($\delta^{15}N$) of various pools of N, combined with the oxygen isotope of NO_3^- ($\delta^{18}O_{NO3}$), has been successfully used to reveal sources and biogeochemical processes of N, especially during the last decade due to significant progress on precise measurements of N and O isotope ratios in seawater [e.g., *Wankel et al.*, 2007; *Dähnke et al.*, 2008; *Chen et al.*, 2013; *Xue et al.*, 2014]. In general, various N sources can be differentiated by their distinct ranges of N and O isotopic values [*Kendall*, 1998, and references therein]. For example, domestic sewage and manure are more enriched in ^{15}N ($\delta^{15}N$: 10–20‰) than fertilizer and atmospheric deposition, and $\delta^{18}O$ values of atmospheric NO_3^- is generally very high (50–80‰) relative to those from other sources (<25‰). However, the applicability of this technique to N source determination in estuaries can be further complicated by biological processes, e.g., assimilation, nitrification, and denitrification, in which significant isotope fractionation may occur due to preferential uptake of lighter isotopes (^{14}N and ^{16}O) [e.g., *Kendall*, 1998; *Casciotti et al.*, 2003]. Thus, a better understanding of N cycling in a coastal marine ecosystem could be achieved by an integrated knowledge of distribution and variation of $\delta^{15}N$ (and $\delta^{18}O$) signatures of various N pools, including dissolved and particulate N.

The Pearl River Estuary (PRE), also known as the Zhujiang Estuary, is an interface connecting south China mainland and the northern South China Sea (NSCS). It is a highly dynamic estuarine system, annually receiving 3.26×10^{11} m^3 of fresh water and 7×10^7 tons of suspended particulate matter (SPM) from the Pearl River, the second largest river in China in terms of flow. Most of the PRE is quite shallow with an average depth of 4.8 m (range from 2 to 10 m). Physical and biogeochemical processes in the PRE show seasonality caused by the regular shift between wet southwesterly monsoon in summer and dry northeasterly monsoon in winter, and thereby, the resultant seasonal variation of river discharge [*Harrison et al*., 2008]. Like many estuarine ecosystems worldwide, the PRE has been dramatically affected by human activities (agriculture, industry, urbanization, etc.) in the Pearl River Delta region over recent decades. Large quantities of biological reactive nitrogen are discharged into the PRE, which in turn lead to environmental problems such as acceleration of eutrophication and formation of hypoxic water [*Huang et al*., 2003; *Dai et al*., 2006].

Extensive effort has been made to understand N origin, distribution, and fate in the PRE, particularly during the wet summer when the input of terrestrial materials is high. There is, however, considerable controversy over whether active N cycling exists in this river-dominated estuary, because mixing diagrams of concentration data versus salinity show a largely conservative behavior [*Yin et al*., 2000; *Cai et al*., 2004] whereas a few shipboard incubation experiments suggest substantial nutrient removal and regeneration (nonconservative) [*Zhang et al*., 1999; *Dai et al*., 2008]. Moreover, there is a shift of nutrient limitation from P to N across the salinity gradient [*Yin et al*., 2001; *Lui and Chen*, 2011]. This shift suggests a more rapid turnover rate of reactive N than P in the PRE, although previous research based on field data observed quite a weak seasonality in some forms of N like NO_3^- [*Zhang et al*., 1999; *Cai et al*., 2004]. Recently, we examined the cycling of reactive N in the PRE during spring by means of NO_3^- dual isotopes ($\delta^{15}N_{NO3}$ and $\delta^{18}O_{NO3}$) and revealed that phytoplankton uptake and microbial nitrification were active under the backdrop of NO_3^- decline due to freshwater-seawater physical mixing [*Ye et al*., 2015]. Taking into account that there are great seasonal contrasts in river discharge and monsoon winds, we thus predicted a remarkable seasonal difference in N dynamics in the PRE, which could be elucidated via isotope analysis of N species.

As compared to our previous research, which studied the spatial N turnover processes (the west and east PRE) during a single season using NO_3^- dual isotopic approach [*Ye et al*., 2015], the present study measured the stable isotopes of dissolved inorganic N (DIN, including NO_3^- and NH_4^+) and particulate N (PN) along a salinity gradient in the PRE to investigate seasonal (winter and summer) variability of N sources and N cycling processes. We found that different degrees of biological processing occurred between the wet and dry periods and that these differences can be traced by $\delta^{15}N$ (and $\delta^{18}O$) of different N species.

2. Materials and Methods

2.1. Field Sampling

Surface samples at 0.5 m depth were collected along a salinity gradient from ~0 to >30.0. The sampling campaigns were conducted in February and August 2014 (Figure 1). The weekly mean river discharges of the Pearl River just prior to our cruises were about 4000 and 15,000 m^3 s^{-1} (http://xxfb.hydroinfo.gov.cn), which was typical for winter and summer, respectively [*Harrison et al*., 2008]. At each sampling station, parameters of water temperature, salinity, and dissolved oxygen (DO) were measured on site. In August 2014, salinity at the outmost site was not high enough to represent typical seawater due to high flux of freshwater; hence, deeper samples (0.5 m above sea bottom) with higher salinities at the two outmost sites were additionally collected.

Temperature and salinity data were recorded using a Valeport CTD meter that was calibrated before the cruise, with precision of ±0.01°C for temperature and ±0.01 for salinity. For collection of suspended particulate matter (SPM), 200–500 ml water samples were filtered on site immediately through precombustion (450°C, 4 h) glass-fiber filters (25 mm diameter, Whatman GF/F). After filtration, the filters were rinsed with Milli-Q water to remove salt and then frozen at −20°C until later analysis for PN concentration and its $\delta^{15}N$. For nutrients as well as NO_3^- and NH_4^+ isotopic analysis, water samples of 500 ml were filtered through precombusted glass-fiber filters (47 mm diameter, Whatman GF/F) and the filtrate was stored at −20°C for home lab analysis in an acid-washed polyethylene bottle. Samples for chlorophyll *a* (Chl *a*) were filtered through 0.7 μm GF/F filter and stored in liquid nitrogen before further processing and analysis.

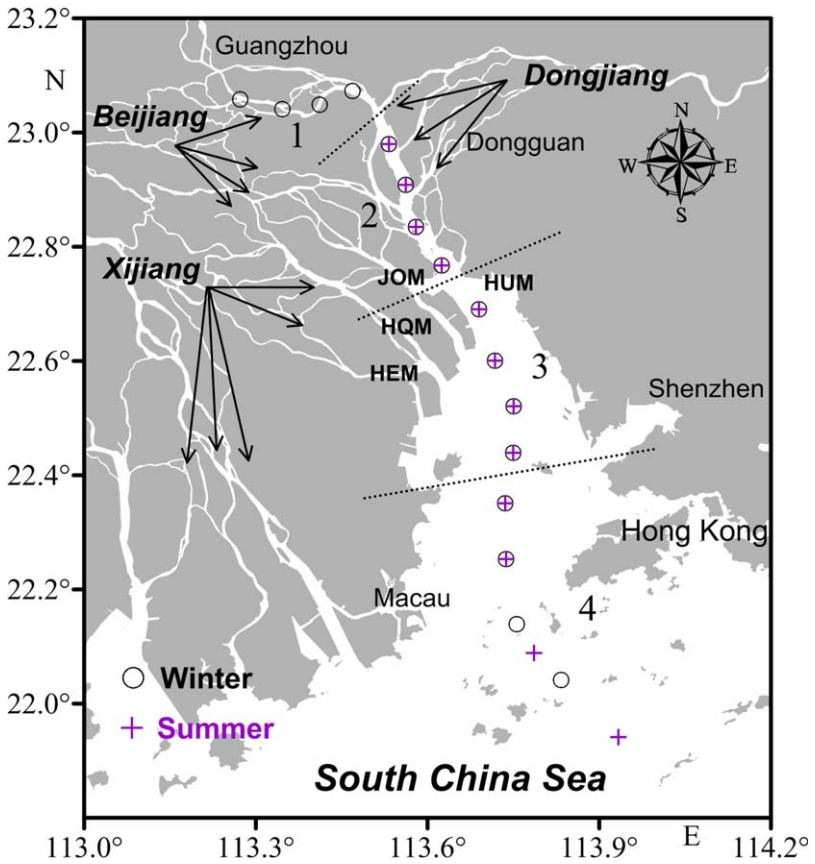

Figure 1. Map of the Pearl River Estuary showing the sampling stations. Four estuarine zones are divided: 1, Guangzhou Channel; 2, upper estuary; 3, middle estuary; and 4, lower estuary. HUM, JOM, HQM, and HEM denote Humen, Jiaomen, Hongqimen, and Hengmen, respectively. The black arrows represent the branches of the three major tributaries.

2.2. Chemical Analyses

Filtered water samples were analyzed for NO_3^-, NO_2^-, and NH_4^+ concentrations using the standard colorimetric procedures that have been fully described elsewhere [*Grasshoff et al*., 1999]. The detection limits for NO_3^-, NO_2^-, and NH_4^+ were 0.05, 0.02, and 0.10 μmol L^{-1}, respectively. Chl *a* concentration in the bulk POM on the GF/F filter was determined spectrophotometrically [*Lorenzen*, 1967].

In home laboratory, SPM filters were oven-dried (50°C for 48 h) and weighed. The weighed differences between the dried filters and their counterparts before filtration were used to calculate SPM. These filters were then acidified with concentrated HCl vapor in a fume hood to remove carbonate, and rinsed with deionized water and redried at 50°C. The filters with decarbonated SPM samples were analyzed for POC and PN contents using an elemental CHNOS analyzer (Elementar Vario) and their isotopic compositions using a Thermo Finnigan isotope ratio mass spectrometer (IRMS) (model: Delta plus XL). Replicate analysis showed that the precision for $\delta^{13}C$ and $\delta^{15}N$ was better than 0.1 and 0.2‰, respectively. Sample acidification could slightly modify the $\delta^{15}N$ value of a sample relative to the untreated sample [*Kennedy et al*., 2005]. However, no difference was detected in the present study between acidified samples and untreated samples based on a sequence comparison of $\delta^{15}N$ data ($n = 8$).

Nitrate $\delta^{15}N$ and $\delta^{18}O$ were measured using the chemical reduction method [*McIlvin and Altabet*, 2005]. Briefly, NO_3^- was reduced to NO_2^- with spongy Cd and NO_2^- was subsequently reduced to N_2O using sodium azide buffered to pH 4–5 using acetic acid. For each sample, preexisting nitrite (NO_2^-) was removed by addition of sulfamic acid, following the procedure of *Granger and Sigman* [2009]. To determine the $\delta^{15}N$ and $\delta^{18}O$ of N_2O, the gas sample was extracted, purified, and analyzed online using a TraceGas inlet coupled to a continuous flow IRMS (GV IsoPrime II). Three international NO_3^- standards (USGS-32, USGS-34, and USGS-35) together with unknowns were measured with each batch of samples and used for isotopic correction.

Isotopic ratios are reported in delta (δ) notation as per mil (‰) relative to atmospheric N_2 (air) for $^{15}N/^{14}N$ and relative to VSMOW (Vienna standard mean ocean water) for $^{18}O/^{16}O$. Analytical precision for international and in-house reference materials was generally better than $\pm 0.3‰$ for $\delta^{15}N$ and $\pm 0.5‰$ for $\delta^{18}O$ ($n = 8$), and the standard deviations for replicate samples were in the same range or better [*Ye et al*., 2015]. Additional samples for NH_4^+ $\delta^{15}N$ analyses were performed according to *Zhang et al*. [2007], which involves oxidizing NH_4^+ to NO_2^- using hypobromite (BrO^-) followed by further reduction to N_2O in the same procedure as described above for $\delta^{15}N_{NO3}$ analyses. Three international NH_4^+ standards (IAEA-N1, USGS-25, and USGS-26) were also used to correct for isotopic fractionation produced during the isotope analysis. Precision of replicate $\delta^{15}N_{NH4}$ analyses of standards was $\pm 0.4‰$.

2.3. Data Analysis

2.3.1. Mixing Calculations

To examine the behavior of various N species along salinity gradient, conservative mixing lines were calculated using the model reported by *Fry* [2002]

$$N_{mix} = q \times N_r + (1-q) \times N_m, \tag{1}$$

where N_r and N_m are the concentration of different N species in riverine and marine end-members, respectively, and q is the freshwater fraction in each sample calculated from salinity

$$q = (S_m - S_{mix})/(S_m - S_r), \tag{2}$$

where S_{mix}, S_m, and S_r are the salinity of a sample, the marine, and riverine end-members, respectively.

In physical mixing, the isotopic value of a sample (δ_{mix}) is the concentration-weighted mean of the isotopic values of riverine and marine end-members.

$$\delta_{mix} = [q \times N_r \times \delta_r + (1-q) \times N_m \times \delta_m]/N_{mix}. \tag{3}$$

Under steady state conditions, the concentration of various N species varies linearly along the mixing gradient, whereas isotopic mixing diagrams show curvilinear mixing behaviors, reflecting the concentration-weighted volumes of the end-members [e.g., *Middelburg and Nieuwenhuize*, 2001; *Fry*, 2002]. In contrast, deviations from the conservative mixing (or nonconservative mixing) lines of concentrations or isotope signatures point toward sources and/or sinks in the mixing gradient.

The choice of end-members is of key importance for the reliability of a mixing model and the subsequent interpretation of isotopic data. Extensive estuarine studies have used sample data at the lowest salinity as the riverine end-member, which is feasible in that there is only one important waterway leading river water into those estuaries [e.g., *Wankel et al*., 2006; *Dähnke et al*., 2008]. However, due to the fact that the Pearl River delta is a complex river network, being fed by three major tributaries and some local runoff with different nutrient levels and dynamics and that all freshwaters were finally discharged into the PRE through four outlets (Figure 1), it is difficult to decide a common freshwater end-member at present. Nevertheless, we adopted an alternative approach that has been successfully used in previous research in this complex estuarine regime [*Guo et al*., 2008; *He et al*., 2010].

Among the four main outlets (i.e., Humen, Jiaomen, Hongqimen, and Hengmen; Figure 1), the two outlets, Humen and Jiaomen, at the top of the PRE discharge the dominant river runoff (~66%) and DIN load (~70%) [*Huang et al*., 2003; *Cai et al*., 2004]. Therefore, values of riverine end-member were fixed by averaging data of the initial fresh-saline mixing water samples from areas that are dominated by river inputs from Humen and Jiaomen. In summer, the mixing mainly occurs at the middle estuary near Humen, whereas in winter, the mixing occurs at the upper Humen area [*Guo et al*., 2008], so we used the water samples from the middle estuary(zone 3) and the upper estuary (zone 2) to obtain the riverine end-member in this study (Table 1). However, we note that these are not truly riverine end-members because they also reflect the influence of multiple N processes that may have occurred in the lower-salinity regions.

It should also be noted that the isotopic values of samples with highest salinities in our study area cannot serve as the marine end-member due to the large spatial variability in $\delta^{15}N$ and $\delta^{18}O$ values in the PRE [*Ye et al*., 2015]. Instead, the relatively stable subsurface water (100–200 m) from the NSCS was applied for the marine end-member (Table 1). This subsurface water is less influenced than other waters by the addition of spatially and temporally variable new sources of N, such as the atmospheric deposition and subsequent

Table 1. Definitions of the Riverine and Marine End-Members

End-Member	Salinity	NO_3^- /PN (μmol L^{-1})	$\delta^{15}N_{NO3}/\delta^{15}N_{PN}$ (‰)	$\delta^{18}O_{NO3}$ (‰)
Winter riverine	5.5	81.8/17.0	−0.9/5.6	2.3
Summer riverine	3.0	70.4/12.7	5.7/10.2	1.6
Marine	34.5	5.0/0.2	4.0/5.0	2.5

biological processes (e.g., algal assimilation and N_2 fixation). Off-shore upwelling in summer [*Ning et al.*, 2004; *Jing et al.*, 2009; *Tang et al.*, 2009] and wind-induced upper water-column mixing in winter [*Tseng et al.*, 2005; *Shen et al.*, 2008; *Wong et al.*, 2015] are the common phenomena in the NSCS, which provides the subsurface nutrients as the ultimate marine end-member for the coastal surface water. In this study, the respective average values previously reported for subsurface water in the NSCS [*Wong et al.*, 2002; *Kao et al.*, 2012; Kao S.-J., N isotopes: implication for nutrient transformation and export productions, unpublished data] were used. Because no marine end-member for $\delta^{15}N$ value of NH_4^+ is available, the mixing line for NH_4^+ isotopes, therefore, was not calculated.

3. Results

3.1. Physiochemical Parameters

Downstream distributions of the physiochemical parameters are shown in Figure 2. Water temperature was low in winter (16.1–18.4°C) and high in summer (27.1–31.9°C). Salinity increased seaward from 0.1 upstream of Humen to >30.0 in the lower estuary, with some slight fluctuations in the middle estuary. Salinity at each site in winter was higher than in summer by 10.6 ± 5.5, with maximal differences in the middle estuary. There was a DO minimum at initial estuarine mixing (salinity <2) in the vicinity of the Humen outlet, that moved downstream in summer relative to its position in winter. Downstream of the DO minimum, a progressive DO increase with increasing salinity was observed in the middle of the estuary (up to 8–10 mg L^{-1}), with higher values in winter than in summer. In high-salinity waters (S > 20), DO showed a slight decreasing trend. SPM and Chl *a* had similar distribution patterns, i.e., they were high at the upstream of the Humen outlet at salinities <1, exhibiting much lower SPM but higher Chl *a* in summer than in winter. Further downstream SPM and Chl *a* generally declined with increasing salinity, except for a secondary maximum at midsalinities during the dry winter, which was likely due to the contribution of local phytoplankton production and/or resuspended sediment particles.

3.2. Nutrient Concentrations

As shown in Figure 3, concentrations of DIN (NO_3^-, NO_2^-, and NH_4^+) and PN varied greatly during both seasons, in good agreement with previous observations in this subtropical estuary [*Zhang et al.*, 1999; *Dai et al.*, 2008]. High level of [NO_3^-] along with high [NH_4^+] occurred in the Guangzhou Channel during winter and in the upper estuary during summer, respectively. All inorganic forms of N decreased rapidly at the early stage of mixing around the Humen outlet, after which they decreased smoothly due to a dilution effect associated with oligotrophic seawater, although there were some remarkable fluctuations (Figures 3a, 3c, 3e, and 3g). The smooth decreasing trend was also shown in the concentration-salinity plots (Figure 3b), where [NO_3^-] was below or varied around the conservative mixing line. In contrast to [NO_3^-], [NH_4^+] was above the conservative mixing in both winter and summer. PN varied similarly to Chl *a* during both wet and dry seasons, showing high concentrations (>30 μmol L^{-1}) in the upper estuary and decreased sharply to values ≤10 μmol L^{-1} in the middle estuary (Figures 3g and 3h). PN was elevated at middle salinity, followed by a moderate decrease further downstream.

3.3. Isotope Compositions

Values of nitrate $\delta^{15}N$ ($\delta^{15}N_{NO3}$) ranged from −2.2 to 10.2‰ (Figures 4a and 4b). They were similar in freshwater (5.3–10.2‰) and seawater (8.6–9.6‰) for both seasons, but on average higher in summer (6.7 ± 1.7‰, n = 14) than in winter (3.2 ± 4.0‰, n = 16) in the estuarine brackish waters. In both seasons, enriched $\delta^{15}N_{NO3}$ (>8.0‰) was coupled with high [NO_3^-] and Chl *a* concentrations, all exhibiting sharp declines downstream at low salinity (S < 2–3). Further downstream, $\delta^{15}N_{NO3}$ remained almost constant during summer (except for the outmost station), but was considerably elevated in winter. Nitrate $\delta^{18}O$ ($\delta^{18}O_{NO3}$) ranged from 0.7 to 25.6‰, with no obvious difference between seasons, except for the lower estuary where exceptional high $\delta^{18}O_{NO3}$ values up to 25.6‰ occurred in winter (Figures 4c and 4d). To our

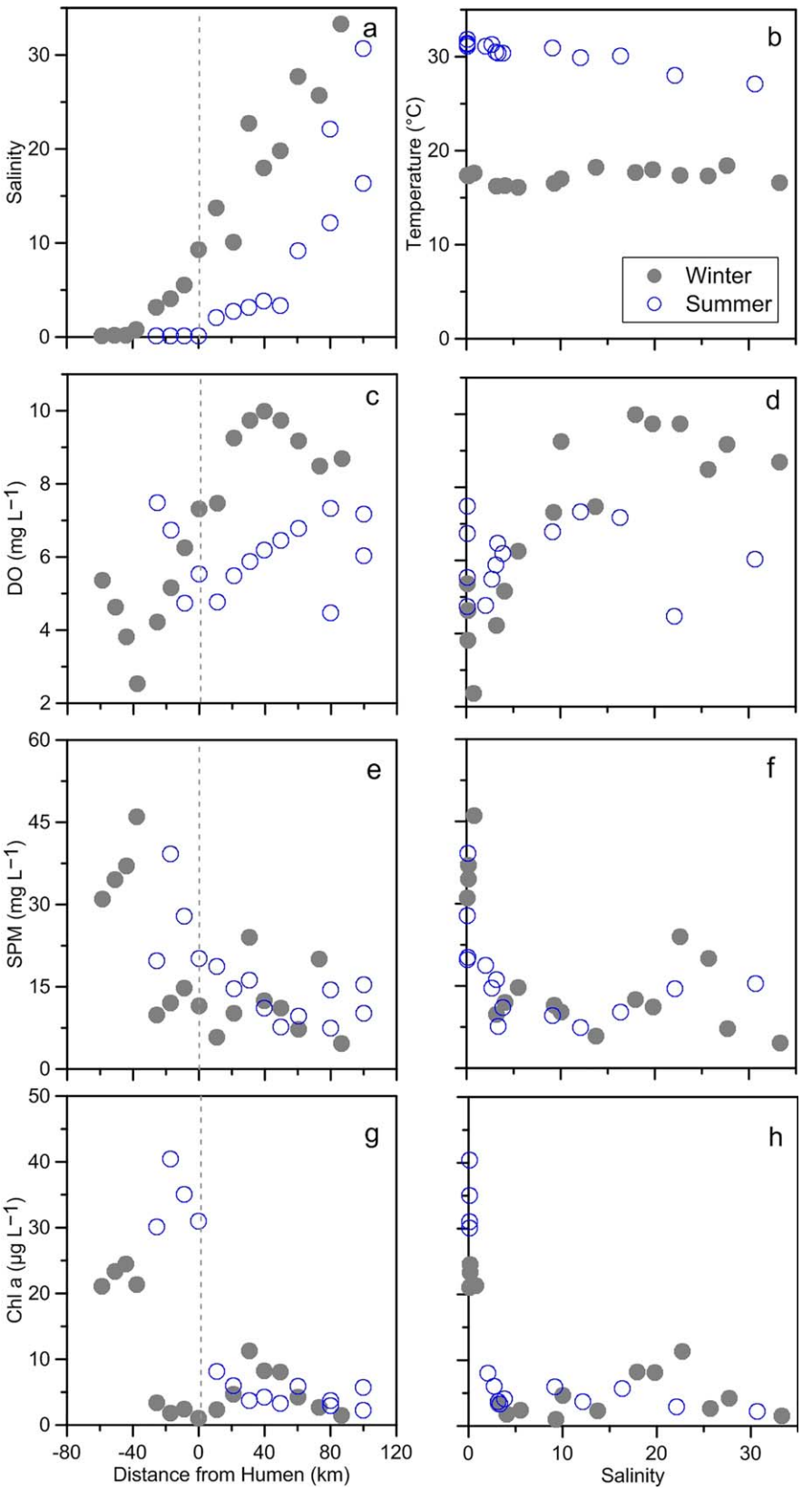

Figure 2. Distribution of salinity, temperature, DO, SPM, and Chl *a* along the sampling transects in the PRE. The left figures are plotted against the distance from Humen and the right ones are plotted against salinity. (a) Salinity; (b) water temperature; (c, d) DO; (e, f) SPM; (g, h) Chl *a*. Gray dashed lines indicate the locations of the Humen outlet.

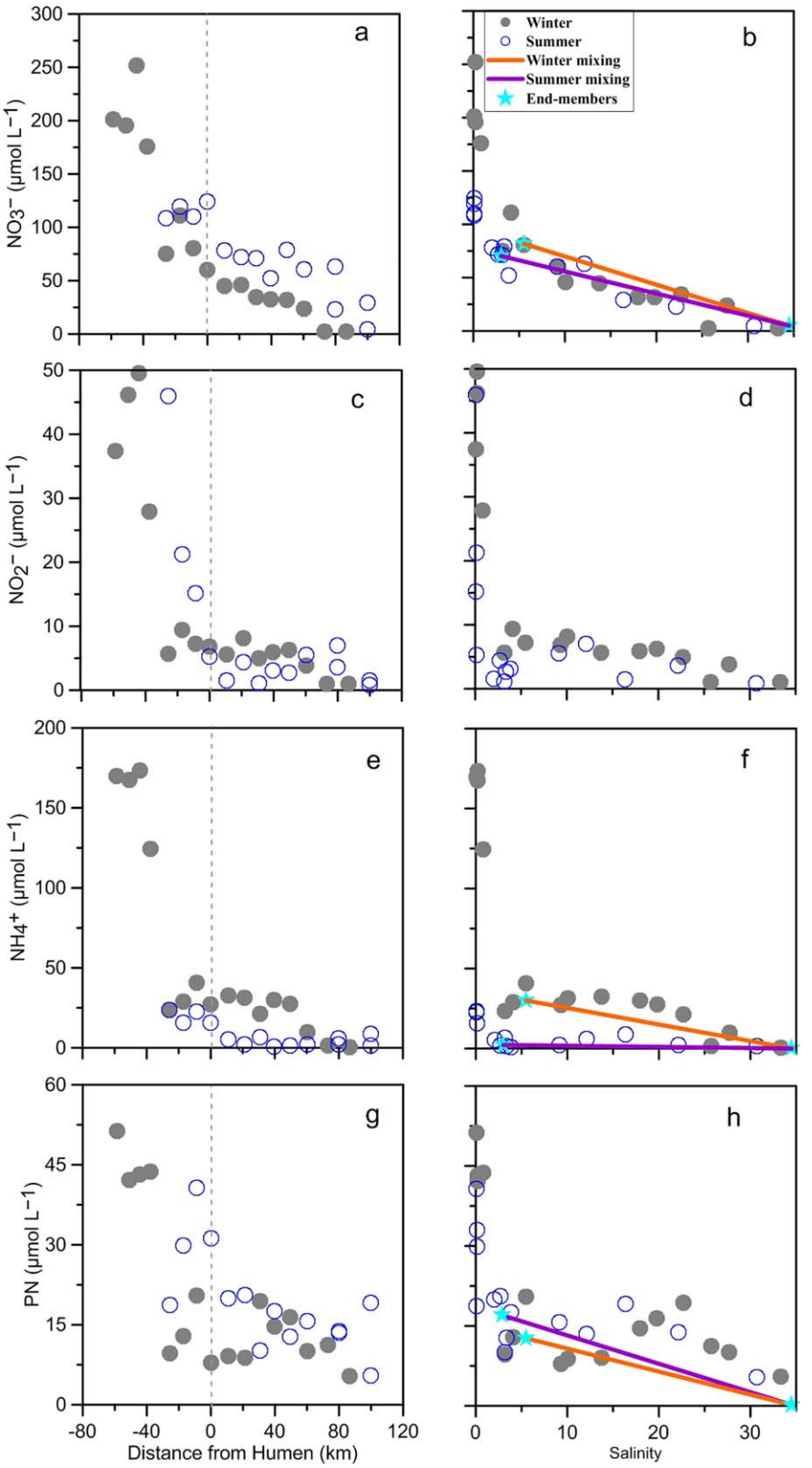

Figure 3. Distribution of NO_3^-, NH_4^+, and PN concentrations along the sampling transects in the PRE. The left figures are plotted against the distance from Humen and the right ones are plotted against salinity: (a, b) NO_3^-; (c, d) NO_2^-; (e, f) NH_4^+; (g, h) PN. Gray dashed lines in left figures indicate the location of the Humen outlet. The stars in right figures denote the freshwater and marine end-members used in this study (for details of the two end-members, see section 2).

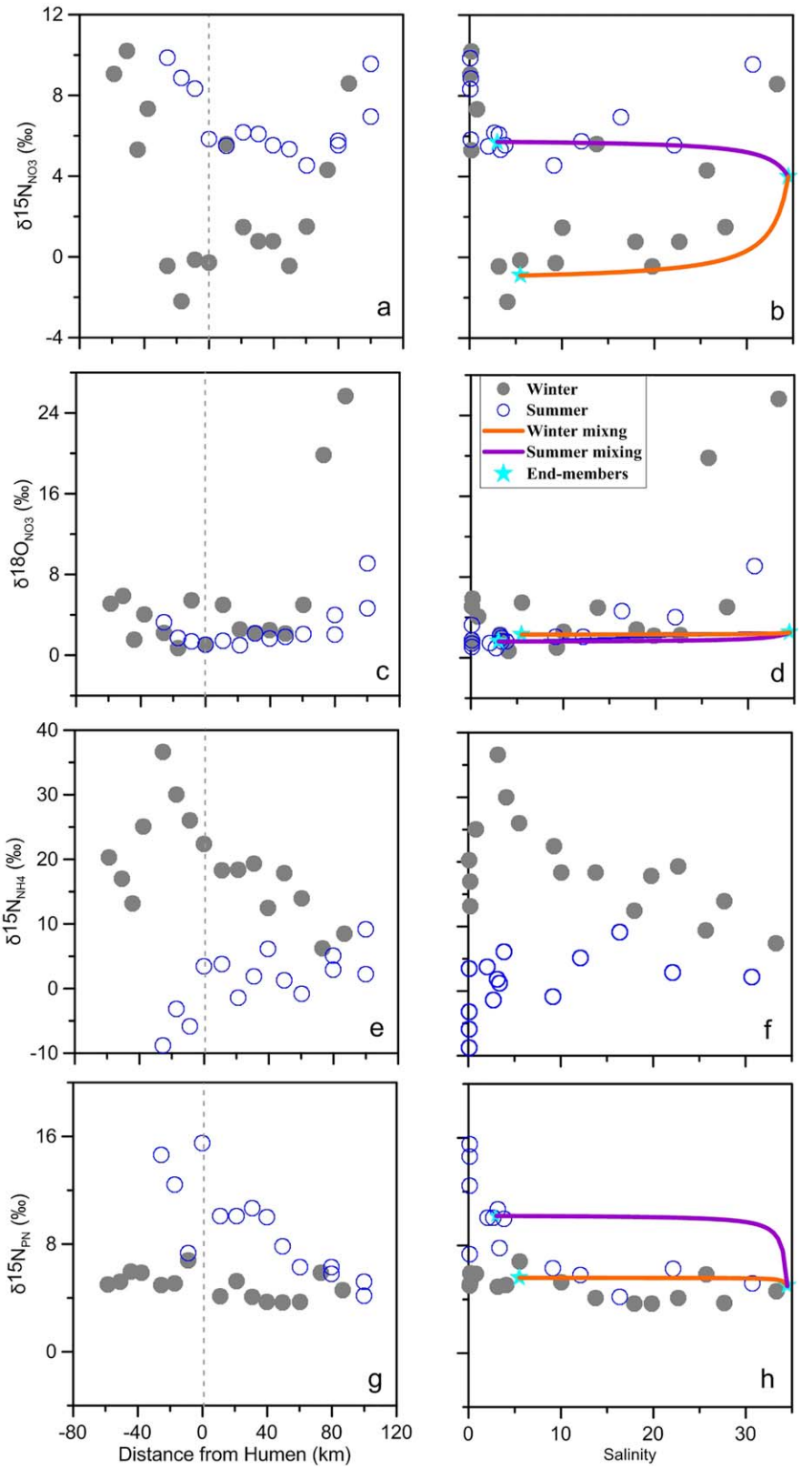

Figure 4. Distribution of $\delta^{15}N_{NO3}$, $\delta^{18}O_{NO3}$, $\delta^{15}N_{NH4}$, and $\delta^{15}N_{PN}$ along the sampling transects in the PRE. The left figures are plotted against the distance from Humen and the right ones are plotted against salinity. The inserted plot Panel i was the concentration-weighted $\delta^{15}N$ values of DIN along with salinity. (a, b) $\delta^{15}N_{NO3}$; (c, d) $\delta^{18}O_{NO3}$; (e, f) $\delta^{15}N_{NH4}$; (g, h) $\delta^{15}N_{PN}$; (i) $\delta^{15}N_{DIN}$. Gray dashed lines in left figures indicate the location of the Humen outlet.

knowledge, the observed $\delta^{18}O_{NO3}$ value is at the high end of the range of $\delta^{18}O_{NO3}$ ever reported in many oceanic environments (−5.0–33.9‰) [e.g., *Wankel et al*., 2006, 2007; *Dähnke et al*., 2008; *Wong et al*., 2014]. Along the salinity gradient, both $\delta^{15}N_{NO3}$ and $\delta^{18}O_{NO3}$ were highly variable at low salinities (S < 2–3) and were more conservative at middle salinities, whereas they were clearly deviated from the mixing line in the high-salinity (S > 20.0) zones.

Ammonium was characterized by a wider range in its $\delta^{15}N$ compared to NO_3^- (Figures 4e and 4f). $\delta^{15}N_{NH4}$ also exhibited strong seasonal differences, with clearly higher values in winter (6.2 to 36.6‰, averaged 19.5‰) than in summer (−8.8 to 9.1‰, averaged 0.9‰) except in the lower PRE. The most remarkable difference occurred in the upper estuary, where $\delta^{15}N_{NH4}$ reached the highest value in winter at a salinity of 3 and lowest value in summer at a salinity of ~0.1. In the salinity range 2–3, there was a sharp increase during both seasons. Thereafter, $\delta^{15}N_{NH4}$ decreased continuously with increasing salinity in winter, whereas it varied between −0.9 and 9.1‰ and showed no clear spatial gradient in summer. Comparatively, the downstream changing pattern of $\delta^{15}N_{NH4}$ largely mirrored that of $\delta^{15}N_{NO3}$.

The $\delta^{15}N$ values of PN ($\delta^{15}N_{PN}$) along the estuary were generally lower in winter (3.7–6.8‰) than in summer (4.2–15.5‰). This seasonal contrast mainly occurred in the upper estuary at salinity <2–3. Downstream of the Humen outlet, $\delta^{15}N_{PN}$ decreased slightly and showed similar values and patterns in summer and winter as salinity increased. For example, a substantial decrease of $\delta^{15}N_{PN}$ was observed in the middle salinity range, followed by a slight increase in the high-salinity waters. This is opposite to the patterns of $\delta^{15}N_{NO3}$ and $\delta^{15}N_{NH4}$ in summer (Figure 4). The $\delta^{15}N_{PN}$-salinity mixing diagram showed nonconservative behavior in summer, with most of the $\delta^{15}N_{PN}$ values below the conservative mixing line. In winter, the $\delta^{15}N_{PN}$ showed nearly conservative behavior throughout the salinity gradient. It is important to note that at middle salinities PN, NO_3^-, and NH_4^+ have very similar $\delta^{15}N$ values in summer, whereas there were large differences among these isotopes in winter, suggesting there is a clear seasonal variation in DIN sources and/or processes within the estuary.

4. Discussion

4.1. Sources of DIN and PN in Freshwater

Sewage effluent has been proposed as a significant source of NO_3^- in the PRE [*Huang et al*., 2003; *Dai et al*., 2008]. Using $\delta^{15}N$ data, we have estimated the relative contribution of this source recently [*Ye et al*., 2015], showing that the contribution of sewage effluent to the total N input to the PRE was 8.3% in average, ranging from 0 to 19%. In the present study, the Guangzhou Channel in winter is characterized by heavier isotopes ($\delta^{15}N_{NO3}$: 5.3–10.2‰ and $\delta^{15}N_{NH4} > 10.0$‰) and higher NO_3^- and NH_4^+ concentrations than the downstream sites (Figures 3 and 4), which are possibly associated with municipal sewage effluents from Guangzhou. In the wet summer, nutrient concentrations were lower in freshwater than those in the dry winter, likely due to dilution by high water discharge (>10,000 $m^3\ s^{-1}$). Nevertheless, they were still quite high (>100 μmol L^{-1}) relative to the downstream brackish waters. Together with higher $\delta^{15}N_{NO3}$ values in freshwater, NO_3^- seems also to be sourced from sewage discharge in summer. However, the concurrent very low $\delta^{15}N_{NH4}$ values (as low as −8.0‰) contradict this source determination. As such, nutrients from catchment soils delivered by runoff and groundwater were likely a candidate. In August, denitrification in the catchment soils has been suggested to occur in the highest degree, causing nitrate $\delta^{15}N$ to be elevated up to 17.6‰ in the tributary of Beijiang River, a major branch of the Pearl River [*Chen et al*., 2009]. Unfortunately, no $\delta^{15}N_{NH4}$ data were reported along with the $\delta^{15}N_{NO3}$ in that study. Nevertheless, due to the extremely low $\delta^{15}N_{NH4}$, we speculate that the cation exchange of NH_4^+ during soil sorption before the NH_4^+ discharge could be partly responsible for this pattern, because ^{15}N is retained preferentially at the exchange site in soil [*Delwiche and Steyn*, 1970]. Indeed, *Koba et al*. [2012] also suggested the importance of cation exchange in the $\delta^{15}N$-depleted NH_4^+ (averaged −9.2‰, ranging from −14.7 to 0.2‰) but positive $\delta^{15}N$ of NO_3^- (0.4–6.8‰) in stream water from an N-saturated subtropical forest nearby the Pearl River Delta. Moreover, nitrogen fertilizer (almost in the reduced form, e.g., urea (71%), NH_4HCO_3 and NH_4Cl (27%), etc.) is heavily applied in the catchment agriculture during the spring and summer times. Ammonium from reduced N fertilizer that was not fully utilized by plants and characterized by low $\delta^{15}N$ values (−5.6 to 1.5‰) might leak and contribute to rivers in this rainy season [*Chen et al*., 2009]. Further investigations are needed to clarify this issue.

At the whole estuary scale, significant positive correlations were found between PN and Chl *a* ($p < 0.01$) during both winter and summer ($r = 0.95$, $n = 16$; $r = 0.83$, $n = 14$, respectively), implying that algal biomass was the major component of PN. The high Chl a concentrations in freshwater perhaps recorded an upper stream (e.g., Beijiang and Dongjiang) signal [*Cai et al*., 2004] and/or likely suggested the importance of in situ phytoplankton production [*He et al*., 2010; *Guo et al*., 2015]. Stable N isotopes can provide additional constraint on the main sources of PN and its subsequent processing. If phytoplankton assimilation is the major control on N isotopic composition of PN, its δ^{15}N should be less than or equal to those of δ^{15}N values of NO_3^- and NH_4^+ depending on relative nutrient utilization as ^{14}N is preferentially assimilated. This is the case for the winter data, in which the δ^{15}N of PN were almost constant (5.0–6.0‰) at salinities <1.0, and were much lower than that of NO_3^- and/or NH_4^+ (Figure 4). However, this did not hold true for summer data, where PN was isotopically heavier (up to 15.5‰) than NO_3^- and NH_4^+. These clearly higher $\delta^{15}N_{PN}$ data were likely caused by the predominant assimilation of NO_3^- that is isotopically enriched [*Li et al*., 2015], rather than NH_4^+, either from upstream or from urban N discharge as discussed earlier. Urban N discharge to the river with an average δ^{15}N of 16‰ has been found to increase river $\delta^{15}N_{PN}$ by 10–15‰ [*Leavitt et al*., 2006]. Moreover, microbial degradation of organic matter (OM) might play a secondary role in causing high $\delta^{15}N_{PN}$ values because microbes preferentially break down the isotopically lighter compounds, which is generally associated with an fractionation factor from −3 to +1‰ [*Kendall et al*., 2007; *Möbius*, 2013].

4.2. Nitrification-Dominated Low-Salinity (<2–3) Waters

Upstream or near the Humen outlet, [NO_3^-] and [NH_4^+] declined greatly from freshwater to low-salinity water (<2–3) during both winter and summer (Figure 3). This decline was much steeper than that occurred in the middle and lower PRE; the latter was obviously caused by dilution by oligotrophic seawater. However, the rapid decline in the low-salinity waters was likely due to dilution of nutrient replete waters from the Guangzhou Channel by numerous less replete stream waters down the channel (Figure 1). For example, the monthly measurements of nutrients in the Jiaomen and Hengmen outlets, which receive the majority freshwater inputs from the Beijiang and a branch of the Xijiang, showed annual averaged concentrations of 68.9 ± 12.4 and 83.6 ± 18.7 μmol L^{-1} for NO_3^-, and 27.2 ± 6.1 and 25.1 ± 13.2 μmol L^{-1} for NH_4^+, respectively [*Lu et al*., 2009]. These values are much lower than that of the Guangzhou Channel, which accounts for only a minor contribution of the total discharge to the PRE (<20%). This occurrence is also believed to be responsible for the sharp decreases in DIC and DOC concentrations in the same region [*Guo et al*., 2008; *He et al*., 2010].

Interestingly, the nutrient decline was accompanied by a significant decrease in $\delta^{15}N_{NO3}$ and increase in $\delta^{15}N_{NH4}$. Although the multiple river inputs and their subsequent mixing were responsible for the sharp decrease in nutrient concentrations, it is unlikely that mixing could abruptly change $\delta^{15}N_{NO3}$ and $\delta^{18}O_{NO3}$ patterns in both seasons. This is mainly due to the fact that other major tributaries of the Pearl River (e.g., the Beijiang and Dongjiang River) are expected to have similar or even higher δ^{15}N as compared to that of the Guangzhou Channel, despite comparatively lower [NO_3^-] [*Chen et al*., 2009; *Li et al*., 2015]. For example, $\delta^{15}N_{NO3}$ in the Beijiang averaged 8.3‰ in winter and 11.8‰ in summer, respectively [*Chen et al*., 2009], whereas the δ^{15}N values of epiphytic algae ranged from 6.7 to 11.2‰ in lower reaches of the Dongjiang, where NO_3^- is found to be the most dominant N form assimilated by these algae [*Li et al*., 2015].

As a result, the close coupling between $\delta^{15}N_{NO3}$ and $\delta^{15}N_{NH4}$ in the low-salinity region, suggests a certain N process, in which NO_3^- and NH_4^+ were closely related with each other. We surmise this process to be most likely water column nitrification, because nitrification in the presence of excess NH_4^+ would result in heavier $\delta^{15}N_{NH4}$ in the residual NH_4^+ pool and add ^{15}N depleted N to the NO_3^- pool [*Mariotti et al*., 1981; *Casciotti et al*., 2003]. Additionally, we found a steady decrease in DO (from 5.4 to 2.5 mg L^{-1} in winter and from 7.5 to 4.7 mg L^{-1} in summer) at salinity <2, which could be closely associated with oxygen demand in nitrification. Previous research has revealed that nitrification could remove one third of the total O_2 in the upper reach of the PRE [*Dai et al*., 2006, 2008]. Intense nitrification has been also noted in estuaries of large rivers receiving substantial NH_4^+ inputs, e.g., the Elbe estuary, the Scheldt estuary and the upper Seine estuary, particularly in the low-salinity region [*de Wilde and de Bie*, 2000; *Sebilo et al*., 2006; *Dähnke et al*., 2008].

Isotope fractionation occurring in a biological system can be approximated by the open-system Rayleigh fractionation that is expressed by the following equation [*Altabet*, 2006]:

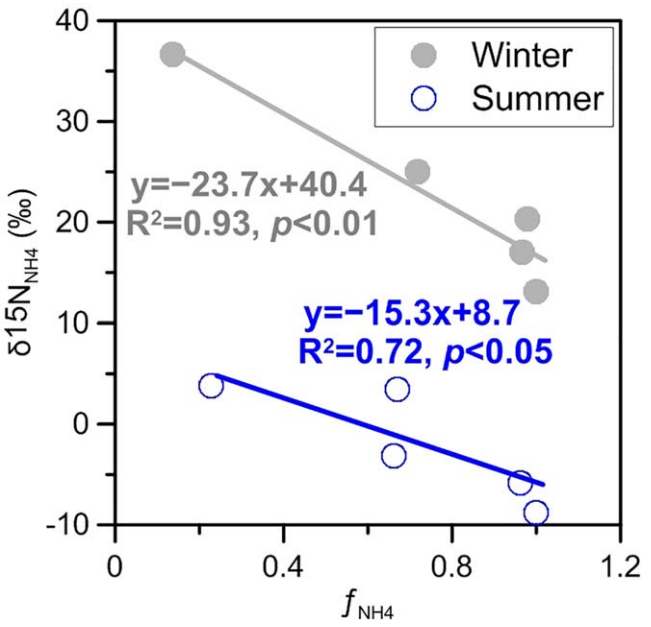

Figure 5. Relationship between $\delta^{15}N_{NH4}$ and f_{NH4} in low-salinity waters.

$$\delta_r = \delta_i + \varepsilon \times f_{NH4}, \quad (4)$$

where δ_r and δ_i are the observed and initial values for isotopic composition of NH_4^+, respectively, ε the fractionation factor, and f_{NH4} the fraction of residual NH_4^+ relative to initial NH_4^+ in the water column ($[NH_4^+]_r/[NH_4^+]_i$). The slopes of the linear regression lines correspond to the N isotope effects of ammonia oxidation in the water column.

In our results, plots of $\delta^{15}N_{NH4}$ versus f_{NH4} showed significant relationships ($p < 0.01$ in winter and $p < 0.05$ in summer, Figure 5) in low-salinity water samples in both summer and winter. The overall estimated ε ($-15.3‰$ in summer and $-23.7‰$ in winter) falls within the reported values for N fractionation factors of field studies (-14 to $-38‰$) [*Casciotti et al.*, 2003]. This finding further supports our argument that microbial nitrification is the primary consumption process of NH_4^+ in low salinities.

However, it should be noted that the extent of $\delta^{15}N_{NO3}$ decrease and $\delta^{15}N_{NH4}$ increase due to the suggested nitrification was smaller in summer than in winter. For example, $\delta^{15}N_{NO3}$ decreased from 5.8–9.9‰ in freshwater to 5.0–6.2‰ in low-salinity waters in summer, whereas the corresponding decrease was from 5.3–10.2‰ to −2.2 to −0.3‰ in winter. For $\delta^{15}N_{NH4}$, the corresponding increase was from −9.3–3.4‰ to −1.4–6.1‰ in summer and from 13.1–25.0‰ to 30.0–38.3‰ in winter. The smaller extent of changes in summer relative to that of winter might be due to the larger freshwater dilution in wet season than in dry season. In addition, because of the short residence times of estuarine waters (<3 days) in the wet season [*Yin et al.*, 2000; *Sun et al.*, 2013], the slow-growing nitrifier populations, with a maximum growth rate of 0.035 to 0.06 h^{-1} [*Brion et al.*, 2000, and references therein], have no time to develop sufficiently to oxidize the available NH_4^+. In contrast, the water residence time was prolonged (~1 week) during the dry season [*Sun et al.*, 2013], which permits nitrifying bacteria to develop a significant biomass in the water column. This general seasonal pattern is consistent with the observations of nitrifier abundance in the PRE [*Dai et al.*, 2008]. In fact, the contrast in water residence time was also suggested to be related to the different degrees of nitrification found between the east and west PRE (Figure 5) [*Ye et al.*, 2015].

Nitrification of NH_4^+ should increase NO_3^- concentrations, which we did not find in winter (Figure 3). Among other processes, denitrification in sediments was at least partially responsible for the lack of NO_3^- increase. The nitrification coupled with denitrification generally leads to losses of N to the atmosphere as N_2O or N_2 [*Herbert*, 1999]. Indeed, *Xu et al.* [2005] and *Dai et al.* [2006] found evidence for a significant loss of water column NO_3^- in winter, which could be directly due to denitrification (rate: 0.03–0.84 mM m^{-2} h^{-1}) occurring in the sediments upstream of the Humen outlet. It is worth noting that the NO_3^- isotope effect of benthic denitrification has been proposed to be significantly less (<−3‰) than that in the water column (−20 to −30‰). The slight increases in $\delta^{15}N$ caused by benthic denitrification could be simultaneously counteracted by the input of low $\delta^{15}N_{NO3}$ from nitrification. Therefore, it is likely that coupled nitrification-denitrification occurred in the low-salinity region, resulting in the decrease of $\delta^{15}N_{NO3}$ values, but without buildup of NO_3^- in winter.

4.3. Water Column N Turnover in Mid and High Salinities

Further downstream in middle and high-salinity waters ($3 < S < 30$), the concentrations and isotopic values of $[NO_3^-]$ and $[NH_4^+]$ along the salinity gradient could suggest conservative freshwater-seawater mixing in the PRE (Figure 3). Previous studies also found evidence of mixing-controlled N distribution in the PRE

based on the concentration data [*Zhang et al*., 1999; *Yin et al*., 2000; *Cai et al*., 2004]. Mixing of the two end-members would also be supported by linear correlation between $\delta^{15}N$ and 1/[N] [*Kendall*, 1998]. However, the lack of linear relationship between either $\delta^{15}N_{NO3}$ and 1/[NO_3^-] or $\delta^{15}N_{NH4}$ and 1/[NH_4^+] in our data ($p > 0.05$, data not shown) implies that such mixing is insufficient to explain the distribution of $\delta^{15}N_{NO3}$ and $\delta^{15}N_{NH4}$ in the PRE during both seasons. This means other biological processes and/or sources with distinct isotopic signatures must be invoked to explain the variations in $\delta^{15}N_{NO3}$ and $\delta^{15}N_{NH4}$ (or $\delta^{15}N_{DIN}$). For example, most data points of [NO_3^-] were distributed below the mixing line, coinciding with ^{15}N-enriched NO_3^-, thus indicating substantial NO_3^- consumption (e.g., assimilation and denitrification) and/or mixing with other sources that are characterized by enriched $\delta^{15}N_{NO3}$ but lower [NO_3^-] relative to the water column (e.g., the interplay between water column and sediment N pools). It should also be noted that PN has very similar $\delta^{15}N$ in both seasons, even though the $\delta^{15}N_{NO3}$ and $\delta^{15}N_{NH4}$ are different between winter and summer.

In winter, there occurred a clear $\delta^{15}N_{NO3}$ increase and $\delta^{15}N_{NH4}$ decrease with increasing salinity. There could be several explanations for the isotope patterns observed, including denitrification, phytoplankton assimilation, and intense physical sediment-water interaction. The influence of local water column denitrification can be ruled out as the cause of the positive $\delta^{15}N_{NO3}$ anomalies because of high DO content in the PRE during winter (Figure 2). DIN assimilation by phytoplankton can cause isotopic enrichment of the residual DIN (NO_3^- and NH_4^+), during which fractionation factors vary among different species [e.g., *Needoba et al*., 2003; *Granger et al*., 2004; *Wankel et al*., 2009; *Wong et al*., 2014]. Indeed, a winter phytoplankton bloom indicated by surface Chl $a > 5.0\ \mu g\ L^{-1}$ and elevated PN concentration had developed in the upper estuary within the salinity range of 15–25 (Figure 2). Along with this bloom, there occurred a pronounced NO_3^- removal (up to 35.3% as calculated by the observed concentrations relative to the calculated mixing line) and slightly enriched $\delta^{15}N_{NO3}$ and $\delta^{18}O_{NO3}$, which may have resulted from NO_3^- assimilation. Moreover, $\delta^{15}N_{PN}$ values also decline at the same time, further linking the isotope anomalies to phytoplankton assimilation. On the basis of the open system model (similar to the one used for nitrification), we calculated a fractionation factor associated with phytoplankton assimilation. In our results, a plot of $\Delta\delta^{15}N$ of NO_3^- (Δ refers to the difference between the observed value and that of expected from conservative mixing) versus f_{NO3} (the fraction of NO_3^- remaining in the system relative to that of expected from conservative mixing) showed a significant relationship ($p < 0.05$) for middle and high-salinity waters in both seasons (Figure 6a). Our estimates yielded ^{15}N fractionation with isotope effects of -4.7 and $-5.1‰$ in summer and winter, falling within the range of reported values (-3 to $-9‰$) for phytoplankton assimilation [*York et al*., 2007]. This suggests that nitrate uptake by phytoplankton played a major role for NO_3^- drawdown and its isotope shifts in these waters, in addition to physical mixing.

However, in the middle salinity waters ($3 < S < 15$), in spite of the NO_3^- isotope anomalies, the effect of assimilation seems insignificant because there was no clear phytoplankton bloom or elevated PN concentration (Figures 2 and 3). Here we tentatively attributed the $\delta^{15}N_{NO3}$ enrichment and concurrent NO_3^- loss

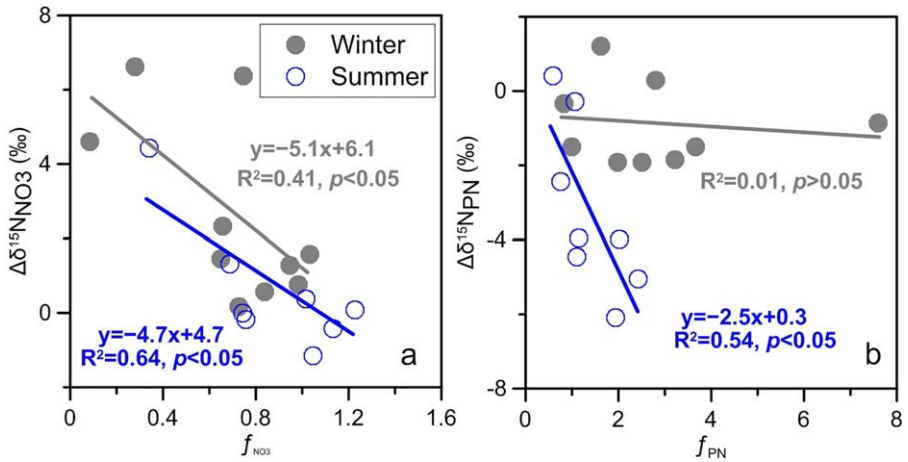

Figure 6. Relationships between (a) nitrate $\Delta\delta^{15}N$ and f_{NO3} and (b) PN $\Delta\delta^{15}N$ and f_{PN} in middle and high-salinity waters of the Pearl River Estuary. $\Delta\delta$ is the difference between the observed isotopic value and that of predicted by the conservative mixing line relating isotopes of a specific N species to salinity.

to the interplay between water and sediment reactive N pools, at least in the region where the largest NO_3^- isotope anomalies were observed. Previous studies found active consumption of NO_3^-, due most likely to denitrification, in the sediments (mostly composed of sand and silt) in the PRE, resulting in efflux of NO_3^- from the water column to the sediments year round [*Zhang et al*., 2013]. If the net flux of NO_3^- is always into the sediment, without advection of NO_3^- out of the sediment, the apparent isotopic N fractionation factor during denitrification will be ~0 [*Brandes and Devol*, 1997; *Lehmann et al*., 2004]. In contrast, if there is an advective flux returning NO_3^- to the overlying water, irrespective of whether through tidal pumping or bioirrigation, $\delta^{15}N$ and $\delta^{18}O$ values of pore water NO_3^- are expected to be substantially high, reflecting more closely the enzyme level N isotopic fractionation by denitrification in the water column [*Wankel et al*., 2009; *Lehmann et al*., 2007]. In the PRE, previous work suggested that biological perturbation, irrigation and other physical perturbation in surface sediments could be very significant, especially during winter when wind-induced mixing and tidal pumping are strong, as evidenced by the large difference between diffusive and incubated fluxes of NO_3^- (up to >2.0 mmol m^{-2} d^{-1} fluxed out of the sediments) [*Pan et al*., 2001; *Zhang et al*., 2013]. Such a dynamic environment would lead to bidirectional exchange of solutes, including NO_3^-, between sediment pore water and the overlying water. This NO_3^- exchange would finally result in elevated $\delta^{15}N_{NO3}$ and $\delta^{18}O_{NO3}$ values but lower [NO_3^-] in estuarine waters due to denitrification-induced isotopic enrichment in sediments. However, this hypothesis will need further evaluation in both field observations and laboratory experiments.

There is no evidence for active NH_4^+ consumption in winter, despite the fact that phytoplankton usually prefer NH_4^+ to NO_3^- due to the overall lower energy cost of assimilation. Instead, most of the middle and high-salinity samples have much lower $\delta^{15}N_{NH4}$ values compared to those expected from conservative mixing, with more depleted $\delta^{15}N_{NH4}$ in response to higher [NH_4^+] (Figures 3 and 4). This pattern suggested the presence of additional NH_4^+ sources. Meanwhile, there occurred a large increase in SPM and PN contents (Figures 2 and 3). So, remineralization of OM in suspended particulates and sediments is a likely source of NH_4^+. In the PRE, the surface sediments and suspended particulates have similar $\delta^{15}N$ values (4.0–6.0‰, Figure 4) [*Hu et al*., 2006]. As OM remineralization is commonly accompanied by only slight isotopic fractionation (−3 to +1‰) [*Kendall et al*., 2007; *Möbius*, 2013], such derived $\delta^{15}N_{NH4}$ could have a value much lower than values from conservative mixing. Indeed, past work in the PRE has shown that significant amounts of NH_4^+ may diffuse from sediments to the overlying waters in both summer and winter due to prolonged degradation of organic matter [*Pan et al*., 2001; *Zhang et al*., 2013]. During winter, the strong wind stress with speeds of 7–10 m s^{-1} and low river discharge may lead to strong vertical mixing of water column and resuspension of particles from bottom sediments, resulting in enhanced vertical flux of NH_4^+, characterized by low $\delta^{15}N$ values, to surface waters [*Harrison et al*., 2008; *Hu and Li*, 2009]. Thus, a significant and continuous contribution of recycled NH_4^+ to the pool of water column NH_4^+ could result in a significant decline in $\delta^{15}N_{NH4}$ along the salinity gradient in winter, as shown in Figure 4.

In contrast to winter, the $\delta^{15}N$ values of both NO_3^- and NH_4^+ in summer were similar to those of PN (4.2–7.8‰) (Figure 4), probably suggesting minimum isotope fractionation during assimilation or a strong coupling between assimilation and remineralization. However, we can rule out the first possibility, because an isotope effect of −2.5‰ was estimated by the linear regression between $\delta^{15}N_{PN}$ and f_{PN} (Figure 6b). More directly, a slight decrease of $\delta^{15}N_{PN}$, accompanied by an increase in $\delta^{15}N$ of both NO_3^- and NH_4^+, likely reflects a pronounced N isotope fractionation during assimilation (i.e., preferential uptake of ^{14}N) in the lower PRE at salinities between 20 and 30. Therefore, the observed pattern is likely due to a tight coupling between assimilation and remineralization. In fact, although NH_4^+ comprises a relatively small fraction of the DIN pool (<10%) in summer, the negative relationship between $\delta^{15}N_{PN}$ and $\delta^{15}N_{NH4}$ (enriched $\delta^{15}N_{NH4}$ but depleted $\delta^{15}N_{PN}$) may suggest active NH_4^+ consumption in warm seasons. This is consistent with the fact NH_4^+ is the preferred N source for most of phytoplankton species. Moreover, phytoplankton also acquired significant N from NO_3^- in summer, as demonstrated by the parallel enrichment of $\delta^{15}N$ and $\delta^{18}O$ in NO_3^-, as well as the somewhat lower [NO_3^-] (Figures 3 and 4). In terms of PN, a large fraction is likely mineralized and recycled before being buried in sediment, which might provide an internal source of NH_4^+ to the water column, as indicated by the slightly higher [NH_4^+] than that of calculated mixing line. The predominant role of PN remineralization in controlling the distribution of NH_4^+ was also evidenced by the significant positive relationship between [NH_4^+] and [PN] ($r = 0.67$, $p < 0.05$). Moreover, the range of $\delta^{15}N_{NH4}$ in summer is rather limited as compared to that of in winter, which might be due to a lack of external NH_4^+ supply and/or

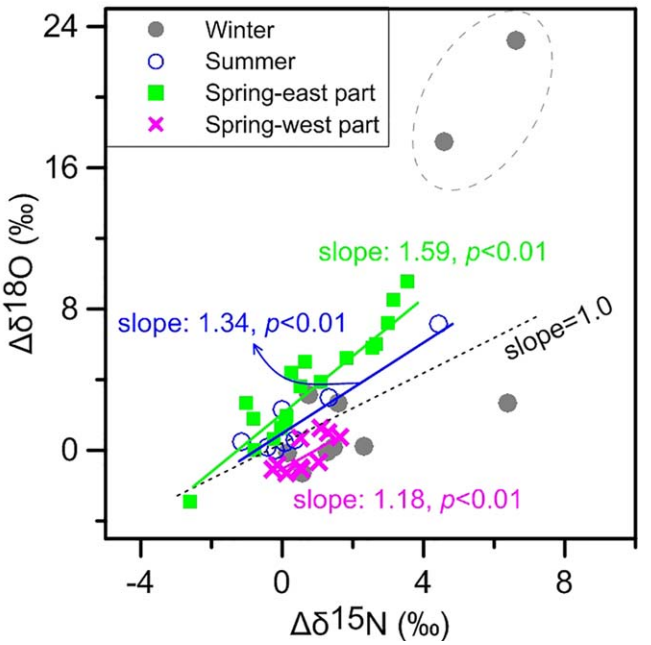

Figure 7. Relationship between nitrate $\Delta\delta^{15}N$ and $\Delta\delta^{18}O$ for the Pearl River Estuary. The dotted line represents a 1:1 ratio. The spring-east part (■) and spring-west part (×) represent the data from the east and west PRE during the spring cruise, respectively [*Ye et al.*, 2015]. The east and west parts of the PRE are divided mainly by the longitudinal deep channel (west channel), where different freshwater inflow and tidal dynamics are expected.

rates of production and consumption are approximately balanced and have similar isotope fractionation factors.

It is noteworthy that $[NH_4^+]$ was quite low (<5 μmol L^{-1}) in the upper PRE, which may contribute little to changes in $\delta^{15}N_{NO3}$ via nitrification, as observed in our sampling area. However, nitrification could still leave isotopic signals, as suggested by the moderate correlation between $\delta^{15}N_{NO3}$ and $\delta^{18}O_{NO3}$ in summer. The correlation showed a slope of 1.34 ($p < 0.01$) in a plot of $\delta^{18}O_{NO3}$ versus $\delta^{15}N_{NO3}$ and deviated from the slope of 1.0 expected from NO_3^- assimilation (Figure 7). This slope value of 1.34 is similar to and within the range of those previously estimated in the west and east PRE during springtime [*Ye et al.*, 2015], indicating there must be other processes/sources that are characterized by relatively depleted $\delta^{15}N_{NO3}$ in addition to isotope mixing and phytoplankton assimilation. The most likely processes are N_2 fixation and nitrification. However, higher N:P ratio values (>16:1) occurring throughout the PRE (data not shown) appear to rule out N_2 fixation as a cause. And thus nitrification may be an important mechanism for generating low $\delta^{15}N_{NO3}$ during summer, particularly over the lower estuary where residence time is prolonged relative to the upper estuary [*Pei et al.*, 2013].

4.4. Atmospheric Deposition as an External NO_3^- Source in High-Salinity Waters

At high salinities (i.e., the lower estuary), $\delta^{15}N_{NO3}$ and $\delta^{18}O_{NO3}$ increased with increasing salinity and deviated clearly from the conservative mixing line (Figure 4). This again confirms that NO_3^- concentrations and its isotopic composition must be greatly impacted by phytoplankton assimilation in the lower estuary, and in good agreement with our previous study [*Ye et al.*, 2015]. However, the extremely high $\delta^{18}O_{NO3}$ and the uncoupling of $\delta^{18}O_{NO3}$ and $\delta^{15}N_{NO3}$ in winter (Figure 4) points to other sources/processes besides assimilation, because assimilation is known to cause equal increases in $\delta^{15}N$ and $\delta^{18}O$ of the residual NO_3^- [*Granger et al.*, 2004]. In addition, we note that neither algal NO_3^- assimilation nor the mixing with other water masses from the NSCS is significant enough to result in high $\delta^{18}O_{NO3}$ values greater than 10‰ [*Ye et al.*, 2015; Kao S.-J., N isotopes: implication for nutrient transformation and export productions, unpublished data]. Therefore, such high values could only be sourced from atmospheric deposition because measured $\delta^{18}O_{NO3}$ values in atmospheric deposition in the NSCS shows an annual average value >50‰ [*Yang et al.*, 2014; *Xiao et al.*, 2015]. Although several studies suggested that most of the atmospheric NO_3^- is likely rapidly recycled in the water column of oligotrophic ocean, the input of atmospheric NO_3^- to surface layer would not be

immediately taken up in the PRE due to a limitation of production by P [*Yin et al.*, 2001; *Harrison et al.*, 2008]. A similar scenario has also been reported in the eastern Mediterranean Sea [*Emeis et al.*, 2010]. Furthermore, the low [NO_3^-] in the lower estuary allows the atmospheric deposition of NO_3^- to be influential on $\delta^{18}O_{NO3}$ values.

In order to quantify the contribution of atmospheric NO_3^- deposition to the dissolved NO_3^- pool, a simple steady state isotope mass balance model based on NO_3^- isotope anomalies, i.e., the deviations from the conservative mixing, was utilized (equations (5) and (6)). Note that the effect of physical mixing between freshwater and seawater is not considered in this model, and as stated above, we assumed that the NO_3^- isotope anomalies are mostly due to phytoplankton assimilation and atmospheric deposition in the lower PRE.

$$\Delta\delta^{15}N_{obs} = \delta^{15}N_{atm} \times N_{atm}/(N_{atm} + N_{mix}) + {}^{15}\varepsilon_{ass} \times f_{NO3}, \quad (5)$$

$$\Delta\delta^{18}O_{obs} = \delta^{18}O_{atm} \times N_{atm}/(N_{atm} + N_{mix}) + {}^{18}\varepsilon_{ass} \times f_{NO3}, \quad (6)$$

where $\Delta\delta^{15}N_{obs}$ and $\Delta\delta^{18}O_{obs}$ represent NO_3^- isotope ($\delta^{15}N_{NO3}$ and $\delta^{18}O_{NO3}$) anomalies relative to those expected from conservative mixing. The first terms on the right hand side of equations (5) and (6) stand for the contribution of atmospheric deposition to δ_{NO3} values, whereas the second terms refer to δ_{NO3} changes associated with NO_3^- assimilation. NO_3^- assimilation by phytoplankton cause equal increases $\delta^{15}N$ and $\delta^{18}O$ (${}^{15}\varepsilon_{ass} = {}^{18}\varepsilon_{ass}$) [*Granger et al.*, 2004]. As a result, by subtracting equation (5) from equation (6), we obtain the following equation:

$$\Delta\delta^{15}N_{obs} - \Delta\delta^{18}O_{obs} = \left(\delta^{15}N_{atm} - \delta^{18}O_{atm}\right) \times N_{atm}/(N_{atm} + N_{mix}). \quad (7)$$

Defining $f_{atm} = N_{atm}/(N_{atm} + N_{mix})$, we have

$$f_{atm} = \left(\Delta\delta^{15}N_{obs} - \Delta\delta^{18}O_{obs}\right)/\left(\delta^{15}N_{atm} - \delta^{18}O_{atm}\right), \quad (8)$$

where f_{atm} is the contribution of atmospheric NO_3^- deposition. Note that this equation is independent of the NO_3^- isotope anomalies due to phytoplankton assimilation, i.e., the second terms in equations (5) and (6). In the present study, the mean $\delta^{15}N$ and $\delta^{18}O$ values of atmospheric NO_3^- ($-2.8‰$ for $\delta^{15}N$ and $58.8‰$ for $\delta^{18}O$) [*Yang et al.*, 2014] observed in the NSCS were used.

Our estimates suggest that the fraction of atmospherically derived NO_3^- in high-salinity waters ranged from 2 to 27% (averaged $17 \pm 13\%$) in winter, with the highest value in the outmost station. In fact, the importance of atmospheric deposition in providing nutrients and metal for new production in the SCS has been noted previously [e.g., *Lin et al.*, 2007; *Yang et al.*, 2014; *Xiao et al.*, 2015]. This takes place particularly during winter when the prevailing northeastern wind can carry anthropogenic particles emitted from, e.g., fossil fuel burning and industrial activities, from mainland China to the NSCS. In summer, wind direction is from the ocean towards land, likely unfavorable for anthropogenic NO_3^- deposition. However, incubation experiments have shown that rainwater that mostly occurs in summer could be an important source to fuel new production in the PRE [*Zhang et al.*, 1999; *Yin et al.*, 2000]. Clearly, future studies with high spatial and temporal resolutions (e.g., monthly) are required to better constrain the importance of atmospheric deposition to surface waters in the study region.

5. Conclusions

Our study on stable isotopes of dissolved and particulate N pools provided detailed information on the biogeochemistry of N in the highly dynamic PRE. We found that the riverine N sources showed marked seasonal variations, with domestic sewage and soil organic N/reduced fertilizer N as the main DIN sources in winter and summer, respectively. At low salinities (<2–3), the influence of nitrification on NO_3^- isotope dynamics was more apparent in winter than in summer, likely related to reduced freshwater dilution in the dry season than in the wet season. In summer, an intrinsic coupling between assimilation and remineralization was inferred from the similar range of $\delta^{15}N$ values of DIN and PN in waters with middle and high salinities. During winter, we stress that the isotopic composition of reactive N at midsalinities is strongly influenced by N cycling at the sediment-water interface. Additionally, our result highlights a significant influence of atmospheric deposition on the NO_3^- pool at high salinities during winter. Together, isotope

data help illustrate a large seasonal variations in the major sources and turnover of reactive N in this subtropical estuary, which are intimately related to human activity and monsoon climate.

Acknowledgments
The authors would like to thank the journal Editor and two anonymous reviewers for their helpful comments. This work is supported by the National Key Research and Development Program (2016YFA0601204), the National Natural Science Foundation of China (41306102 and 41276072), and partially supported by the Open Foundation of State Key Laboratory of Tropical Oceanography (LTO1306). This is contribution IS-2311 from GIGCAS. To access the data published in this manuscript, refer to the corresponding author (jiagd@gig.ac.cn).

References

Altabet, M. A. (2006), Isotopic tracers of the marine nitrogen cycle: Present and past, in *The Handbook of Environmental Chemistry. Marine Organic Matter: Chemical and Biological Markers*, vol. 2, edited by O. Hutzinger, pp. 251–294, Springer, Berlin.

Brandes, J. A., and A. H. Devol (1997), Isotopic fractionation of oxygen and nitrogen in coastal marine sediments, *Geochim. Cosmochim. Acta*, *61*, 1793–1801.

Brion, N., G. Billen, L. Guezennec, and A. Ficht (2000), Distribution of nitrifying activity in the Seine River (France) from Paris to the estuary, *Estuaries*, *23*, 669–682.

Cai, W. J., M. Dai, Y. Wang, W. Zhai, T. Huang, S. Chen, F. Zhang, Z. Chen, and Z. Wang (2004), The biogeochemistry of inorganic carbon and nutrients in the Pearl River estuary and the adjacent Northern South China Sea, *Cont. Shelf Res.*, *24*, 1301–1319.

Casciotti, K. L., D. M. Sigman, and B. B. Ward (2003), Linking diversity and stable isotope fractionation in ammonia-oxidizing bacteria, *Geomicrobiol. J.*, *20*(4), 335–353.

Chen, F., G. D. Jia, and J. Chen (2009), Nitrate sources and watershed denitrification inferred from nitrate dual isotopes in the Beijiang River, south China, *Biogeochemistry*, *94*, 163–174.

Chen, F., J. Chen, G. Jia, H. Jin, J. Xu, Z. Yang, Y. Zhuang, X. Liu, and H. Zhang (2013), Nitrate δ^{15}N and δ^{18}O evidence for active biological transformation in the Changjiang Estuary and the adjacent East China Sea, *Acta Oceanol. Sin.*, *32*, 11–17.

Dähnke, K., E. Bahlmann, and K. Emeis (2008), A nitrate sink in estuaries? An assessment by means of stable nitrate isotopes in the Elbe estuary, *Limnol. Oceanogr.*, *53*, 1504–1511.

Dai, M., X. Guo, W. Zhai, L. Yuan, B. Wang, L. Wang, P. Cai, T. Tang, and W.-J. Cai (2006), Oxygen depletion in the upper reach of the Pearl River estuary during a winter drought, *Mar. Chem.*, *102*, 159–169.

Dai, M., L. Wang, X. Guo, Q. Li, B. He, and S.-J. Kao (2008), Nitrification and inorganic nitrogen distribution in a large perturbed river/estuarine system: The Pearl River Estuary, China, *Biogeosciences*, *5*, 1227–1244.

Delwiche, C. C., and P. L. Steyn (1970), Nitrogen isotope fractionation in soils and microbial reactions, *Environ. Sci. Technol.*, *4*, 929–935.

de Wilde, H. P. J., and M. J. M. de Bie (2000), Nitrous oxide in the Schelde estuary: Production by nitrification and emission to the atmosphere, *Mar. Chem.*, *69*, 203–216.

Emeis, K.-C., P. Mara, T. Schlarbaum, J. Möbius, K. Dähnke, U. Struck, N. Mihalopoulos, and M. Krom (2010), External N inputs and internal N cycling traced by isotope ratios of nitrate, dissolved reduced nitrogen and particulate nitrogen in the eastern Mediterranean Sea, *J. Geophys. Res.*, *115*, G04041, doi:10.1029/2009JG001214.

Fry, B. (2002), Conservative mixing of stable isotopes across estuarine salinity gradients: A conceptual framework for monitoring watershed influences on downstream fisheries production, *Estuaries*, *25*, 264–271.

Granger, J., and D. M. Sigman (2009), Removal of nitrite with sulfamic acid for nitrate N and O isotope analysis with the denitrifier method, *Rapid Commun. Mass Spectrom.*, *23*, 3753–3762.

Granger, J., D. M. Sigman, J. A. Needoba, and P. J. Harrison (2004), Coupled nitrogen and oxygen isotope fractionation of nitrate during assimilation by cultures of marine phytoplankton, *Limnol. Oceanogr.*, *49*, 1763–1773.

Grasshoff, K., K. Kremling, and M. Ehrhardt (1999), *Methods of Seawater Analysis*, Wiley-VCH, Weinheim, Germany.

Guo, W., F. Ye, S. Xu, and G. Jia (2015), Seasonal variation in sources and processing of particulate organic carbon in the Pearl River estuary, South China, *Estuarine Coastal Shelf Sci.*, *167*, 540–548.

Guo, X., W.-J. Cai, W. Zhai, M. Dai, Y. Wang, and B. Chen (2008), Seasonal variations in the inorganic carbon system in the Pearl River (Zhujiang) estuary, *Cont. Shelf Res.*, *28*, 1424–1434.

Harrison, P.J., K. Yin, J.H.W. Lee, J. Gan, and H. Liu (2008), Physical-biological coupling in the Pearl River Estuary, *Cont. Shelf Res.*, *28*, 1405–1415.

He, B., M. Dai, W. Zhai, L. Wang, K. Wang, J. Chen, J. Lin, A. Han, and Y. Xu (2010), Distribution, degradation and dynamics of dissolved organic carbon and its major compound classes in the Pearl River estuary, China, *Mar. Chem.*, *119*, 52–64.

Herbert, R. A. (1999), Nitrogen cycling in coastal marine ecosystems, *FEMS Microbiol. Rev.*, *23*, 563–590.

Hu, J., and S. Li (2009), Modeling the mass fluxes and transformations of nutrients in the Pearl River Delta, China, *J. Mar. Syst.*, *78*, 146–167.

Hu, J., P. Peng, G. Jia, B. Xian, and G. Zhang (2006), Distribution and sources of organic carbon, nitrogen and their isotopes in sediments of the subtropical Pearl River estuary and adjacent shelf, South China, *Mar. Chem.*, *98*, 274–285.

Huang, X. P., L. M. Huang, and W. Z. Yue (2003), The characteristics of nutrients and eutrophication in the Pearl River estuary, South China, *Mar. Pollut. Bull.*, *47*, 30–36.

Jing, Z., Y. Qi, Z. Hua, and H. Zhang (2009), Numerical studies on the summer upwelling system in the northern continental shelf of the South China Sea, *Cont. Shelf Res.*, *29*, 467–478.

Kao, S.-J., J.-Y.T. Yang, K.-K. Liu, M. Dai, W.-C. Chou, H.-L. Lin, and H. Ren (2012), Isotope constraints on particulate nitrogen source and dynamics in the upper water column of the oligotrophic South China Sea, *Global Biogeochem. Cy.*, *26*, GB2033, doi:10.1029/2011GB004091.

Kendall, C. (1998), Tracing sources and cycling of nitrate in catchments, in *Isotope Tracers in Catchment Hydrology*, edited by C. Kendall and J. J. McDonnel, Elsevier, New York.

Kendall, C., E. M. Elliott, and S. D. Wankel (2007), Tracing anthropogenic inputs of nitrogen to ecosystems, in *Stable Isotopes in Ecology and Environmental Science*, edited by R. H. Michener and K. Lajtha, pp. 375–449, Blackwell Sci. Publ., Oxford, U. K.

Kennedy, P., H. Kennedy, and S. Papadimitriou (2005), The effect of acidification on the determination of organic carbon, total nitrogen and their stable isotopic composition in algae and marine sediment, *Rapid Commun. Mass Spectrom.*, *19*, 1063–1068.

Koba, K., et al. (2012), The ^{15}N natural abundance of the N lost from an N-saturated subtropical forest in southern China, *J. Geophys. Res.*, *117*, G02015, doi:10.1029/2010JG001615.

Leavitt, P. R., C. S. Brock, C. Ebel, and A. Patoine (2006), Landscape-scale effects of urban nitrogen on a chain of freshwater lakes in central North America, *Limnol. Oceanogr.*, *51*, 2262–2277.

Lehmann, M. F., D. M. Sigman, and W. M. Berelson (2004), Coupling the ^{15}N/^{14}N and ^{18}O/^{16}O of nitrate as a constraint on benthic nitrogen cycling, *Mar. Chem.*, *88*, 1–20.

Lehmann, M. F., D. M. Sigman, D. C. McCorkle, J. Granger, S. Hoffmann, G. Cane, and B. G. Brunelle (2007), The distribution of nitrate ^{15}N/^{14}N in marine sediments and the impact of benthic nitrogen loss on the isotopic composition of oceanic nitrate, *Geochim. Cosmochim. Acta*, *71*, 5384–5404.

Li, X., et al. (2015), Temporal-spatial distribution and source of nitrogen in main stem of Dongjiang River [in Chinese with English abstract], *Acta Sci. Circumstantiae*, *35*, 2143–2149.

Lin, I.-I., J.-P. Chen, G. T. F. Wong, C.-W. Huang, and C.-C. Lien (2007), Aerosol input into the South China Sea: Results from the Moderate resolution imaging spectro-radiometer, the quick scatterometer, and the measurements of pollution in the troposphere sensor, *Deep Sea Res., Part II*, *54*, 1589–1601.

Lorenzen, C. J. (1967), Determination of chlorophyll and pheopigments: Spectrophotometric equations, *Limnol. Oceanogr.*, *12*, 343–346.

Lu, F. H., H. G. Ni, F. Liu, and E. Y. Zeng (2009), Occurrence of nutrients in riverine runoff of the Pearl River Delta, South China, *J. Hydrol.*, *376*, 107–115.

Lui, H. K., and C. T. A. Chen (2011), Shifts in limiting nutrients in an estuary caused by mixing and biological activity, *Limnol. Oceanogr.*, *56*, 989–998.

Mariotti, A., J. C. Germon, P. Hubert, P. Kaiser, R. Letolle, A. Tardieux, and P. Tardieux (1981), Experimental determination of nitrogen kinetic isotope fractionation: Some principles; Illustration for the denitrification and nitrification processes, *Plant Soil*, *62*, 413–430.

McIlvin, M. R., and M. A. Altabet (2005), Chemical conversion of nitrate and nitrite to nitrous oxide for nitrogen and oxygen isotopic analysis in freshwater and seawater, *Anal. Chem.*, *77*, 5589–5595.

Middelburg, J. J., and J. Nieuwenhuize (2001), Nitrogen isotope tracing of dissolved inorganic nitrogen behavior in tidal estuaries, *Estuarine Coastal Shelf Sci.*, *53*, 385–391.

Möbius, J. (2013), Isotope fractionation during nitrogen remineralization (ammonification): Implications for nitrogen isotope biogeochemistry, *Geochim. Cosmochim. Acta*, *105*, 422–432.

Needoba, J. A., N. A. Waser, P. J. Harrison, and S. E. Calvert (2003), Nitrogen isotope fractionation in 12 species of marine phytoplankton during growth on nitrate, *Mar. Ecol. Prog. Ser.*, *255*, 81–91.

Ning, X., F. Chai, H. Xue, Y. Cai, C. Liu, and J. Shi (2004), Physical-biological oceanographic coupling influencing phytoplankton and primary production in the South China Sea, *J. Geophys. Res.*, *109*, C10005, doi:10.1029/2004JC002365.

Pan, J., H. Zhou, X. Liu, C. Hu, L. Dong, and M. Zhang (2001), Nutrient profiles in interstitial water and flux in water-sediment interface of the Zhujiang Estuary of China in summer, *Acta Oceanol. Sin.*, *20*, 523–533.

Pei, M., S. Li, J. Hu, and X. Hu (2013), Simulation of the water exchange in the Pearl River Estuary during wet and dry seasons [in Chinese with English abstract], *J. Trop. Oceanogr.*, *32*(6), 28–35.

Sebilo, M., G. Billen, B. Mayer, D. Billiou, M. Grably, J. Garnier, and A. Mariotti (2006), Assessing nitrification and denitrification in the Seine river and estuary using chemical and isotopic techniques, *Ecosystems*, *9*, 564–577.

Shen S., G. G. Leptoukh, J. G. Acker, Z. Yu, and S. J. Kempler (2008), Seasonal variations of chlorophyll a concentration in the northern South China Sea, *IEEE Geosci. Remote Sens. Lett.*, *5*, 315–319.

Sun, J., B. Lin, K. Li, and G. Jiang (2013), A modelling study of residence time and exposure time in the Pearl River Estuary, China, *J. Hydroenviron. Res.*, *8*, 1–11.

Tang, L., J. Sheng, X. Ji, W. Cao, and D. Liu (2009), Investigation of three dimensional circulation and hydrology over the Pearl River Estuary of China using a nested-grid coastal circulation model, *Ocean Dyn.*, *59*, 899–919.

Tseng, C. M., G. T. F. Wong, I. I. Lin, C. R. Wu, and K. K. Liu (2005), A unique seasonal pattern in phytoplankton biomass in low-latitude waters in the South China Sea, *Geophys. Res. Lett.*, *32*, L08608, doi:10.1029/2004GL022111.

Wankel, S. D., C. Kendall, C. A. Francis, and A. Paytan (2006), Nitrogen sources and cycling in the San Francisco Bay Estuary: A nitrate dual isotopic composition approach, *Limnol. Oceanogr.*, *51*(4), 1654–1664.

Wankel, S. D., C. Kendall, J. T. Pennington, F. P. Chavez, and A. Paytan (2007), Nitrification in the euphotic zone as evidenced by nitrate dual isotopic composition: observations from Monterey Bay, California, *Global Biogeochem. Cycles*, *21*, GB2009, doi:10.1029/2006GB002723.

Wankel, S. D., C. Kendall, and A. Paytan (2009), Using nitrate dual isotopic composition (δ^{15}N and δ^{18}O) as a tool for exploring sources and cycling of nitrate in an estuarine system: Elkhorn Slough, California, *J. Geophys. Res.*, *114*, G01011, doi:10.1029/2008JG000729.

Wong, G. T. F., S. W. Chung, F. K. Shiah, C. C. Chen, L. S. Wen, and K. K. Liu (2002), Nitrate anomaly in the upper nutricline in the northern South China Sea-evidence for nitrogen fixation, *Geophys. Res. Lett.*, *29*(23), 2097, doi:10.1029/2002GL015796.

Wong, G. T. F., X. Pan, K. Y. Li, F. K. Shiah, T. Y. Ho, and X. Guo (2015), Hydrography and nutrient dynamics in the Northern South China Sea Shelf-sea (NoSoCS), *Deep Sea Res., Part II*, *117*, 23–40.

Wong, W. W., M. R. Grace, I. Cartwright, and P. L. M. Cook (2014), Sources and fate of nitrate in a groundwater-fed estuary elucidated using stable isotope ratios of nitrogen and oxygen, *Limnol. Oceanogr.*, *59*, 1493–1509.

Xiao, H.-W., et al. (2015), Use of isotopic compositions of nitrate in TSP to identify sources and chemistry in South China Sea, *Atmos. Environ.*, *109*, 70–78.

Xu, J., Y. Wang, Q. Wang, and J. Yin, (2005), Nitrous oxide concentration and nitrification and denitrification in Zhujiang River Estuary, China, *Acta Oceanol. Sci.*, *24*, 122–130.

Xue, D., P. Boeckx, and Z. Wang (2014), Nitrate sources and dynamics in a salinized river and estuary—A δ^{15}N–NO_3^- and δ^{18}O–NO_3^- isotope approach, *Biogeosciences*, *11*, 5957–5967.

Yang, J. Y. T., S. C. Hsu, M. H. Dai, S. S. Y. Hsiao, and S. J. Kao (2014), Isotopic composition of water-soluble nitrate in bulk atmospheric deposition at Dongsha Island: Sources and implications of external N supply to the northern South China Sea, *Biogeosciences*, *11*, 1833–1846.

Ye, F., Z. Ni, L. Xie, G. Wei, and G. Jia (2015), Isotopic evidence for the turnover of biological reactive nitrogen in the Pearl River Estuary, south China, *J. Geophys. Res. Biogeosci.*, *120*, 661–672, doi:10.1002/2014JG002842.

Yin, K., P. Y. Qian, J. C. Chen, D. P. H. Hsieh, and P. J. Harrison (2000), Dynamics of nutrients and phytoplankton biomass in the Pearl River estuary and adjacent waters of Hong Kong during summer: Preliminary evidence for phosphorus and silicon limitation, *Mar. Ecol. Prog. Ser.*, *194*, 295–305.

Yin, K., P. Y. Qian, M. C. S. Wu, J. C. Chen, L. Huang, X. Song, and W. Jian (2001), Shift from P to N limitation of phytoplankton growth across the Pearl River estuarine plume during summer, *Mar. Ecol. Prog. Ser.*, *221*, 17–28.

York, J. K., G. Tomasky, I. Valiela, and D. J. Repeta (2007), Stable isotopic detection of ammonium and nitrate assimilation by phytoplankton in the Waquoit Bay estuarine system, *Limnol. Oceanogr.*, *52*, 144–155.

Zhang, J., Z. G. Yu, J. T. Wang, J. L. Ren, H. T. Chen, H. Xiong, L. X. Dong, and W. Y. Xu (1999), The subtropical Zhujiang (Pearl River) Estuary: Nutrient, trace species and their relationship to photosynthesis, *Estuarine Coastal Shelf Sci.*, *49*, 385–400.

Zhang, L., M. A. Altabet, T. Wu, and O. Hadas (2007), Sensitive measurements of $NH_4^{+15}N/^{14}N$ ($\delta^{15}NH_4^+$) at natural abundance levels in fresh and saltwaters, *Anal. Chem.*, *79*, 5297–5303.

Zhang, L., L. Wang, K. Yin, Y. Lü, D. Zhang, Y. Yang, and X. Huang (2013), Pore water nutrient characteristics and the fluxes across the sediment in the Pearl River estuary and adjacent waters, China, *Estuarine Coastal Shelf Sci.*, *133*, 182–192.